
Research Article: New Research | Cognition and Behavior

Effects of neuron shutter observed in the EEG alpha rhythm

<https://doi.org/10.1523/ENEURO.0171-20.2020>

Cite as: eNeuro 2020; 10.1523/ENEURO.0171-20.2020

Received: 30 April 2020

Revised: 8 September 2020

Accepted: 10 September 2020

This Early Release article has been peer-reviewed and accepted, but has not been through the composition and copyediting processes. The final version may differ slightly in style or formatting and will contain links to any extended data.

Alerts: Sign up at www.eneuro.org/alerts to receive customized email alerts when the fully formatted version of this article is published.

Copyright © 2020 Alexander et al.

This is an open-access article distributed under the terms of the Creative Commons Attribution 4.0 International license, which permits unrestricted use, distribution and reproduction in any medium provided that the original work is properly attributed.

- 1 **1) Manuscript Title:** Effects of neuronc shutter observed in the EEG alpha rhythm
2
3 **2) Abbreviated Title:** Neuronc shutter in EEG alpha
4
5 **3) Authors:** Kevin E. Alexander¹, Justin R. Estep^{2,1}, and Sherif M. Elbasiouny^{3,1}
6 **Affiliation:** ¹Department of Biomedical, Industrial, and Human Factors Engineering, College of
7 Engineering and Computer Science, Wright State University, Dayton, OH 45435, United
8 States
9 ²711th Human Performance Wing, Air Force Research Laboratory, Wright-Patterson AFB,
10 OH 45433, United States
11 ³Department of Neuroscience, Cell Biology, and Physiology, Boonshoft School of Medicine
12 and College of Science and Mathematics, Wright State University, Dayton, OH 45435,
13 United States
14
15 **4) Author Contributions:** KA, JE, and SE designed research; KA performed research and analyzed data;
16 KA, JE, and SE wrote the paper.
17 **5) Corresponding Author:** Sherif M. Elbasiouny, PhD, PE
18 3640 Colonel Glenn Hwy, 350 NEC Bldg.
19 Dayton, OH 45435 USA
20 Phone: 937-775-2492
21 Email: sherif.elbasiouny@wright.edu
22
23 **6) # of Figures:** 11 **9) # of words in Abstract:** 236 / 250
24 **7) # of Tables:** 2 **10) # of words in Significance Statement:** 103 / 120
25 **8) # of Multimedia:** 0 **11) # of words in Introduction:** 739 / 750
26 **12) # of words in Discussion:** 2036 / 3000
27
28 **13) Acknowledgements:** none
29
30 **14) Conflict of Interest:** Authors report no conflict of interest.
31
32 **15) Funding Sources:** Funding for this work was provided to SME by: (1) Ball Aerospace under contract
33 to the U.S. Air Force, (2) the U.S. National Institute of Health–National Institute of Neurological
34 Disorders and Stroke (NINDS) and National Institute on Aging (NIA) grant # NS091836, and (3) the
National Academy of Sciences (NAS) and the United States Agency for International Development
(USAID), NAS Subaward No: 2000009148. Any opinions, findings, conclusions, or recommendations
expressed in this article are those of the authors alone, and do not necessarily reflect the views of USAID
or NAS.

35 **Abstract**

36 The posterior alpha rhythm, seen in human electroencephalogram (EEG), is posited to originate from
37 cycling inhibitory/excitatory states of visual relay cells in the thalamus. These cycling states are thought
38 to lead to oscillating visual sensitivity levels termed the “neuronic shutter effect.” If true, perceptual
39 performance should be predictable by observed alpha phase (of cycling inhibitory/excitatory states)
40 relative to the timeline of afferentiation onto the visual cortex. Here, we tested this hypothesis by
41 presenting contrast changes at near perceptual threshold intensity through closed eyelids to 20 participants
42 (balanced for gender) during times of spontaneous alpha oscillations. To more accurately and rigorously
43 test the shutter hypothesis than ever before, alpha rhythm phase and amplitude were calculated relative to
44 each individual’s retina-to-V1 conduction delay, estimated from the individual’s C1 visual-evoked
45 potential latency. Our results show that stimulus observation rates are greater at a trough than a peak of
46 the posterior alpha rhythm when phase is measured at the individual’s conduction delay relative to
47 stimulus onset. Specifically, the optimal phase for stimulus observation was found to be 272.41° , where
48 observation rates are 20.96% greater than the opposing phase of 92.41° . The perception-phase
49 relationship is modulated by alpha rhythm amplitude and is not observed at lower amplitude oscillations.
50 Collectively, these results provide support to the “neuronic shutter” hypothesis and demonstrate a phase
51 and timing relationship consistent with the theory that cycling excitability in the thalamic relay cells
52 underly posterior alpha oscillations.

53 **Significance Statement**

54 After accounting for neural conduction delays, we found that threshold intensity stimuli are observed at
55 higher rates when the alpha wave is at a trough phase than at a peak phase, but only when alpha amplitude
56 is high. Our results were derived using methods consistent with a specific hypothesis about a mechanism
57 of visual perception, considering the structure, physiology, and transmission delays in the visual system.
58 The results of this rigorous study design add support to the neuronal shutter hypothesis and are consistent
59 with the theory that posterior alpha reflects cycling excitability in thalamic relay cells, thereby gating the
60 flow of visual information.

61 **Introduction**

62 The posterior alpha rhythm, a 7-13Hz oscillation, is a notable characteristic of the human EEG over the
63 occipital cortex, especially when eyes are closed (Berry and Wagner, 2015). This is thought to assist
64 attention regulation, as its characteristics are often found to correlate with attention over specific sensory
65 cortices (Sauseng et al., 2005; Ben-Simon et al., 2013) – possibly a gating mechanism to limit the flow of
66 sensory information (Cooper et al., 2003; Janssens et al., 2018). This rhythm has analogs in the
67 sensorimotor (Pineda, 2005; Bazanov and Vernon, 2014) and auditory cortices (Tiihonen et al., 1991;
68 Weisz et al., 2011), with both appearing to provide similar gating. This regulatory function is further
69 demonstrated by the observation that alpha activity increases during introspective behavior (Ancoli and
70 Green, 1977) and behaviors involving internally directed attention such as imagination (Cooper et al.,
71 2003), mental arithmetic (Ray and Cole, 1985), autobiographical recall (Yue et al., 2013), and meditative
72 practices (Tenke et al., 2017) presumably because external sensory information is distractive during these
73 behaviors.

74 However, the cellular mechanism and functional significance of alpha oscillations remains unclear. In the
75 1950's, alpha oscillations were proposed to represent a 'neuronic shutter' (Callaway and Alexander,
76 1960) to down-sample incoming sensory information to reduce processing load, and similar discrete
77 perceptual processes are proposed today (VanRullen and Koch, 2003; VanRullen et al., 2014). This
78 shutter is thought to occur at the lateral geniculate nucleus (LGN), which relays visual information to V1.
79 At times, LGN relay cells burst-fire at 10Hz, with a hyperpolarized refractory period between bursts
80 (Lopes da Silva, 1991; Sherman, 2001; Timofeev and Bazhenov, 2005; Alexander et al., 2006; Timofeev
81 and Chauvette, 2011). If many of these cells fire synchronously, visual afferentation during a widespread
82 refractory period is less likely to be relayed to V1, resulting in a 10Hz visual shutter. Each burst in LGN
83 relay cells results in a large excitatory postsynaptic potential (EPSP) at V1, measured as a negativity in
84 the occipital EEG (Timofeev and Bazhenov, 2005), with higher amplitudes indicating more synchronous
85 excitation (Pfurtscheller et al., 1996) resulting, as hypothesized by this model, from LGN excitatory

86 volleys. Thus, the alpha rhythm is thought to reflect cycling excitability in the LGN visual-relay cells,
87 which would result in cycling visual sensitivity in phase with the alpha oscillation. Evidence of this
88 mechanism producing alpha oscillations has been found in animal models with the associated phasic
89 gating of sensory transfer ([Lorincz et al., 2009](#); [Chen et al., 2016](#)). The hypothesis of the present study
90 was based on this model; however, we did not directly test the underlying cellular mechanism.

91 To more accurately measure the alpha phase relationship to perceptual performance, we accounted for
92 neural conduction delays: If a stimulus strikes the retina at t_0 , that information arrives at the LGN at a
93 later time, t_1 . Therefore, the t_1 LGN excitatory state determines whether the information is relayed to V1.
94 Further, the LGN excitatory state is measurable even later in the EEG, as V1 EPSPs at t_2 . Thus, t_0 to t_2
95 represents the retina-to-V1 conduction delay: At t_2 , we can *assess* the t_1 LGN excitability, the time of
96 afferentation of the t_0 stimulus. This is the first study, to our knowledge, to directly examine the
97 relationship between visual observation and spontaneous alpha phase relative to each individual's
98 conduction delay, which advances the accuracy and rigor for testing the shutter hypothesis.

99 This study's objective is to more robustly test the hypothesis that posterior alpha reflects cyclic
100 excitability of the visual system with a phase and timing relationship predicted by underlying
101 physiological model and conduction delays. Therefore, we presented visual stimuli (t_0) to participants
102 during spontaneous occipital alpha activity, then measured alpha amplitude and phase at t_2 (estimated by
103 the individual's C1 visual-evoked potential component peak latency) ([Di Russo et al., 2001](#)). We
104 predicted that visual stimuli at t_0 would be more likely observed with alpha phase at a trough at t_2
105 (assumed to indicate t_1 LGN excitation) than at a peak (t_1 LGN inhibition). Additionally, this effect was
106 predicted to be greater at high alpha amplitudes, indicating greater cellular excitatory state synchrony. We
107 found that participants responded to 20.96% more stimuli with alpha phase at a trough vs. a peak at t_2
108 when alpha amplitude was high. At low amplitude, no significant phase effect on observation rate was
109 observed. These results support our hypothesis that the alpha rhythm reflects cyclic excitatory states in the
110 visual system resulting in a visual shutter effect.

111 **Materials & Methods**

112

113 **Participants:** Alpha activity varies largely both within ([Gonçalves et al., 2006](#)) and between ([Wieneke et](#)
114 [al., 1980](#)) individuals. For this study, we needed to ensure stimuli were able to be presented during times
115 of observable (e.g., stationary) alpha oscillations and therefore selected participants who more readily and
116 reliably generated observable occipital alpha activity. This selection was made by observing EEG activity
117 as the participants practiced the visual sensitivity task with eyes closed during an earlier portion of the
118 experimental session. Participants who did not readily and reliably produce occipital alpha oscillations
119 during this practice period were excluded from further participation.

120 In total, 41 participants were recruited for this study. Based on the observable alpha criteria described
121 above, 21 participants were excluded from further participation. The remaining 20 healthy participants
122 (10 males/10 females, mean age: 22.3 years, range: 18-28 years) completed two tasks: one to estimate
123 their individual conduction delay; the other to investigate their visual sensitivity at different phases of
124 alpha oscillations. The experimental protocol was approved by the Institutional Review Boards of Wright
125 State University and the Air Force Research Laboratory. All participants were compensated for their time.

126

127 **Recording:** All recordings were made using the BioSemi ActiveTwo system (BioSemi B.V., Amsterdam,
128 The Netherlands). Recordings were made with a 2048 Hz sampling rate at 64 channel locations based on
129 the modified combinatorial nomenclature extension of the 10-10 system ([American](#)
130 [Electroencephalographic Society, 1994](#)) excluding the inferior chain with the exception of P9/P10 and Iz
131 ([Seeck et al., 2017](#)), with bilateral electrodes on the mastoid process, infraorbital, and outer canthus
132 locations. Participant responses were recorded using a low-latency mechanical keyboard (Cherry MX 6.0
133 [G80-3930], Cherry GmbH, Auerbach in der Oberpfalz, Germany). This was combined with other task-

134 state and visual-stimulus timing information via light sensors placed on the monitor to record events on
135 the ActiveTwo's 16-bit trigger line (StimTracker 1G, Cedrus Corporation, San Pedro, California, USA).

136

137 **Stimuli:** All tasks and stimuli were constructed and presented using MATLAB (R2011b; The MathWorks,
138 Inc., Natick, MA, USA) and the Psychophysics Toolbox (v3.0.13) ([Brainard, 1997](#); [Pelli, 1997](#); [Kleiner et
139 al., 2007](#)). This software was run on a Dell Precision T3610 computer (Dell Inc., Round Rock, TX, USA)
140 with the Windows 7 Professional operating system (Microsoft Corporation, Redmond, WA, USA).
141 Stimuli were presented to participants on a 24.5", 240 Hz monitor (BenQ ZOWIE XL2540, BenQ
142 Corporation, Taipei, Taiwan) providing 4.2 ms temporal resolution for stimulus presentation. Where
143 relevant, stimulus luminance was measured using a light meter (Light Meter LUX/FC 840020, SPER
144 SCIENTIFIC, Scottsdale, AZ, USA). The participant's head position was fixed using a chinrest placed 58
145 cm from this monitor. The experiment was conducted in a dark room with a natural sound machine
146 (Dohm Classic, Marpac LLC, Wilmington, NC, USA) to mask noise disturbances.

147

148 **Data Analysis:** All data analyses were performed in MATLAB (R2019b; The MathWorks, Inc., Natick,
149 MA, USA) utilizing the EEGLAB Toolbox (v2019.0) ([Delorme and Makeig, 2004](#)) and the ERPLAB
150 plugin (v7.0.0) ([Lopez-Calderon and Luck, 2014](#)). Statistical analyses were conducted using MATLAB's
151 Statistics and Machine Learning Toolbox (R2019b; The MathWorks, Inc., Natick, MA, USA). This
152 software was run on a Lenovo ThinkPad P50 computer (Lenovo, Quarry Bay, Hong Kong) with the
153 Windows 10 Enterprise operating system (Microsoft Corporation, Redmond, WA, USA).

154 **Code Accessibility:** Task design and data analysis code are made publicly available at <https://osf.io/qnryf/>
155 DOI: 10.17605/OSF.IO/QNRYF in addition to the recorded EEG data.

156 *Estimation of t_2*

157 The peak latency of each participant's C1 visual-evoked potential (VEP) component was used as an
158 estimate of their individual retina-to-V1 conduction delay, t_2 . This component reflects the arrival of a
159 volley of visual information to V1 from the LGN along the optic radiations. This is analogous to the alpha
160 wave, in the sense that it also reflects excitatory burst volleys from the LGN to V1, according to the
161 hypothesized model. The C1 peak, rather than onset, latency was used to estimate the middle point of
162 these volleys rather than their onset. Due to the specific folding of the V1 cortical area around the
163 calcarine fissure (Figure 1A), the C1 wave shape will vary with the location of the stimulus in the visual
164 field. Stimuli presented horizontally centered in the visual field will stimulate spatially opposing V1
165 neurons whose dipoles will cancel each other out, yielding no measurable C1 component in the EEG
166 (Clark et al., 1995; Di Russo et al., 2001). This is similarly the case for stimuli presented approximately
167 3° below the vertical center (Clark et al., 1995; Di Russo et al., 2001). However, with some horizontal
168 spacing, bilateral stimuli presented above -3° in the visual field will produce a negative C1 wave, while
169 those presented below -3° in the visual field will produce a positive C1 wave as shown in Figure 1B
170 (Clark et al., 1995; Di Russo et al., 2001).

171 C1 waves are found to be measured maximally at electrode POz using an averaged mastoid reference, but
172 they are still quite small in amplitude. To obtain a well-defined C1 VEP component, both negative and
173 positive components were obtained using upper and lower visual field stimuli. Next, the difference
174 between these two signals was taken to create a large-amplitude wave with a clear peak (Figure 1C shows
175 these waveforms from a single participant). This peak latency was taken as an estimate of t_2 .

176

177 **Experimental Design:** The stimulus used for this task was a 17° wide, 6.38° tall black and white
178 checkerboard made of 16x6 1.06° squares placed on an otherwise black screen with a fixation point
179 placed in the center (Figure 1B). The checkerboard was flashed with its center either 5° above or 7.5°

180 below the fixation point and centered horizontally. The size and placement of these stimuli were selected
181 to generate maximum amplitude waves (Clark et al., 1995). A total of 600 upper and 600 lower stimuli
182 were presented in a mixed random order each with a duration of 33 ms with random 250-450 ms
183 interstimulus-intervals, resulting in a trial time of approximately 7.5 minutes.

184 Similarly to Di Russo et al. (2001), participant attention and gaze were maintained on the fixation point
185 by a sham task performed during the trial. The fixation point would occasionally flash to a brighter color
186 for 12.6 ms, and the participant was instructed to watch for this flash and to respond by pressing the space
187 bar.

188

189 **Analysis:** For the C1 VEP analysis, the originally recorded 2048 Hz sampling rate was maintained but re-
190 referenced to averaged mastoids. All EEG signals were band-pass filtered from 0.01 to 50 Hz at -6 dB,
191 using a 2nd order IIR Butterworth filter as implemented in the ERPLAB toolbox (Lopez-Calderon and
192 Luck, 2014), to achieve a zero-phase filter response. A bipolar vertical electrooculogram (vEOG) signal
193 was created by subtracting the averaged left and right infraorbital electrodes from the averaged Fp1 and
194 Fp2 electrodes.

195 The data were epoched from 50 ms prior to 200 ms after stimulus presentation for both the upper and
196 lower visual stimuli. Blinks within these epochs were detected by sliding a 150 ms window at 75 ms steps
197 over the vEOG signal, and any window containing a peak-to-peak amplitude of 100 μ V or greater was
198 rejected from analysis. Separate average VEPs were calculated for the upper and lower stimulus trials and
199 were baseline-corrected to the 50 ms pre-stimulus period. The lower visual field VEP was then subtracted
200 from the upper field VEP to create a difference wave containing a C1 wave with a clear peak.

201 The C1 peak latency was measured at electrode POz by finding the most negative peak within the 0-110
202 ms time window relative to stimulus onset. This peak latency was calculated for each participant
203 individually and was used as an estimate of their individual t_2 .

204

205 ***Measuring Observation Rates***

206 This task was designed to be conducted with closed eyes in order to evoke more frequent (Legewie et al.,
207 1969) and higher amplitude alpha oscillations (Barry et al., 2007). For this purpose, stimuli were designed
208 such that they could be observed as light flashes through closed eyelids. The brightness of these flashes
209 was designed to be near threshold intensity (where participants reported seeing approximately 50% of the
210 stimuli) to prevent any ceiling or floor effects on performance.

211

212 ***Experimental Design:***The stimulus used for this task was an 8.5° square centered on an otherwise black
213 (0.7 lux) screen. The stimulus brightness was defined by coloring the square as a greyscale value from 0
214 (completely black; 0.7 lux) to 255 (completely white; 89.2 lux). The stimulus was designed to be
215 observable through the closed eyes of the participant. The brightness of the stimulus was adjusted to near
216 the threshold intensity for each individual participant, the value at which the participant reported
217 observing the stimulus half of the number of times it was presented. This threshold was estimated using
218 the staircase method as described in Cornsweet (1962) during a calibration task prior to the main task. In
219 this task, the participant kept their eyes closed as a series of flashes were presented, each time the
220 participant reported observing a flash (using the spacebar) the stimulus intensity was decreased in the next
221 trial. However, if the participant did not report observing the stimulus, the intensity was increased on the
222 next trial. Following the methods described in Cornsweet (1962), threshold intensity is defined as the
223 average of all trials following the third reversal in trial-intensity slope. An example of this task from one

224 participant is shown in Figure 2. In this figure, the third reversal occurred at trial 5, and threshold
225 intensity was calculated as the average of trials 6 to 40.

226 The stimuli used were so dim that the participants' ability to perceive them was sensitive to how well
227 their eyes had adapted to the dark. Pilot testing of the task revealed that, without an adjustment period, the
228 threshold brightness found during the calibration task would become easier to see over the course of the
229 main task. Although visual adaptation to the dark will continue over many hours, the most rapid changes
230 occur in the first 15 minutes, and visual acuity begins to plateau in 20 minutes ([Bierings et al., 2018](#)).
231 Therefore, participants were given 25 minutes in the dark as an adaptation period before conducting the
232 calibration task to estimate the threshold brightness.

233 In the main task, the stimuli were flashed for a period of 8.4 ms and the participant was instructed to
234 respond using the keyboard any time they observed a flash. The participant had to respond with the space
235 bar within two seconds of the stimulus to be a valid response. The experimenter triggered the stimuli
236 during the times of occipital alpha oscillation as observed in the real-time data throughout the task. After
237 the experimenter triggered the stimulus, it was presented after a random interval of less than 750 ms (to
238 mitigate potential confounding effects experimenter bias in stimulus presentation timing).

239

240 **Analysis:**All data were down-sampled to 512 Hz and re-referenced to averaged mastoids. The signal was
241 bandpass filtered from 0.01 to 50 Hz at -6dB using a 2nd order IIR Butterworth filter, as implemented in
242 the ERPLAB toolbox ([Lopez-Calderon and Luck, 2014](#)), to achieve a zero-phase filter response. A
243 bipolar vEOG signal was created by subtracting the averaged left and right infraorbital electrodes from
244 the averaged Fp1 and Fp2 electrodes.

245 To isolate the activities of the left and right visual cortices, a left occipital (LO) signal was calculated by
246 averaging the channels O1, PO3, and PO7, and a right occipital (RO) signal was calculated by averaging

247 channels O2, PO4, and PO8. LO and RO were then convolved with a 10 Hz complex Morlet wavelet to
248 obtain time-domain power and phase signals (Cohen, 2014). A peak-to-peak amplitude signal was then
249 calculated by doubling the square root of the power signal.

250 The Morlet wavelet was constructed with a center frequency of 10 Hz containing $2^{2/3}$ cycles (the
251 recommended minimum (Cohen, 2019)). This cycle count was chosen to optimize temporal resolution
252 and resulted in a wavelet with a full-width at half maximum (FWHM) of 101.6 ms in the time domain and
253 8.87 Hz in the frequency domain. A FWHM of 8.87 Hz indicates that the wavelet convolution was
254 effectively a bandpass filter with half-power points of 5.57 and 14.44 Hz, approximating the alpha
255 frequency band.

256 The following analysis was then performed independently for each participant. Amplitude and phase were
257 measured from LO and RO at the individuals' t_2 relative to stimulus onset for both observed and missed
258 trials. Trials in which LO and RO phases differed by more than 90° were rejected from further analysis to
259 control for alpha asynchrony between the hemispheres. For each of the remaining trials, a single
260 amplitude and phase value was obtained by averaging the amplitude and phase of the LO and RO signals.
261 Phase values were averaged using appropriate statistics for circular quantities (Berens, 2009). These trials
262 were then divided by median amplitude into high and low amplitude bins and then further divided by
263 phase using 90° bins centered on 0° , 90° , 180° , and 270° phase angles. The amplitude median was chosen
264 to provide equal sample sizes in each amplitude bin, and since it is appropriate regardless of distribution
265 normality. When the individual amplitude distributions of our 20 subjects were examined, they appeared
266 to be unimodal and approximately normal with no point of division appearing to be more advantageous
267 than the median (see Figure 3). Observation rates (OR, the percentage of trials in which the participant
268 observed the stimulus) were then calculated for every bin, and the overall OR across all bins (i.e., the
269 average OR over all trials) was subtracted from these values to obtain a Δ OR value for each of the 2
270 (amplitude) x 4 (phase) bins. Note that Δ OR is not a measure of percent change, but simply a difference
271 of the overall OR and the condition specific OR.

272

273 ***Statistical Analysis:*** This analysis resulted in a within-subjects 2x4 repeated measures design with twenty
274 participants and two factors: amplitude (high, low) and phase (0°, 90°, 180°, 270°). These data were
275 analyzed using a repeated measures ANOVA, testing both main effect of amplitude and phase as well as
276 their interaction. Independent t-test and Tukey's HSD tests were used to probe any effects found to be
277 significant. All statistical analyses were conducted using MATLAB's Statistics and Machine Learning
278 Toolbox (R2019b; The MathWorks, Inc., Natick, MA, USA).

279 **Results**

280 ***Individual retina-to-V1 conduction delay (t_2) measurement***

281 In the first part of the experiment, the goal was to estimate each participant's retina-to-V1 conduction
282 delay, t_2 . To calculate that, we measured in each participant the averaged VEPs in response to upper and
283 lower visual stimuli and calculated the "difference waveform" (based on the difference between two
284 signals); the peak latency of this difference waveform was taken as the participant's t_2 (Figure 4). The
285 mean t_2 for all participants was 75.56 ms (range = [62.99, 88.87] ms, 95% confidence interval (CI) =
286 [72.44, 78.69] ms). These data indicate that it takes, on average, 75.56 ms for visual information to be
287 transmitted from the retina to area V1. For each participant, the phase and amplitude measurements were
288 made at the individual's t_2 relative to the stimulus onset to assess visual sensitivity.

289

290 ***Observation rate measurement***

291 The second part of the experiment aimed to investigate if perceptual performance, when measured at t_2 , is
292 higher at an alpha wave trough (i.e., phase angle of 270°) than an alpha wave peak (i.e., phase angle of
293 90°). To examine this, we presented light flashes to each participant through closed eyes. Light flashes
294 were near individual threshold intensity estimated using the staircase method ([Cornsweet, 1962](#)) during a
295 calibration task prior to the main task to prevent ceiling and floor performance effects. This resulted in the
296 stimuli of average luminance across participants of 6.48 lux. Use of these near-threshold stimuli resulting
297 in total observation rates averaging 58.28% across participants.

298 On average, participants were presented 161.65 stimuli during the main task (range = [120, 200]) with an
299 average interstimulus interval of 12.52 seconds. Left occipital (LO) and right occipital (RO) amplitude
300 and phase signals were measured for each participant and analyzed at the participant's t_2 time point.
301 Trials in which LO and RO phases differed by more than 90° were rejected from further analysis resulting
302 in 135.75 trials remaining per participant on average (range = [85, 183]). The amplitude measures were
303 split by their median value into two bins (high and low), and the phase measures were split into four 90°

304 bins centered on 0°, 90°, 180°, and 270° phase angles. A within-subjects 2 (amplitude) x 4 (phase)
 305 repeated measures ANOVA analysis was conducted on the participant Δ OR values (calculated as the OR
 306 per bin minus the overall OR). Mauchly tests indicated no significant violation in the assumption of
 307 sphericity for phase ($\chi^2(5) = 10.169, p = 0.0706$), or the interaction of phase and amplitude ($\chi^2(5) = 3.250,$
 308 $p = 0.6615$). The ANOVA analysis showed that phase and the interaction between phase and amplitude
 309 have statistically significant effects on observation rates, as shown in Table 2. Accordingly, these
 310 ANOVA results support our hypothesis that a relationship between alpha phase and visual observation
 311 exists, and that this relationship is modulated by the alpha wave amplitude.

Table 1. Two (amplitude) x Four (phase) within-subjects repeated measures ANOVA results.

Source	Statistic	p	η_p^2	Power
phase	$F(3,57) = 7.971$	0.0002	0.2955	0.986
amplitude	$F(1,19) = 1.751$	0.2014	0.0844	0.242
phase*amplitude	$F(3,57) = 3.770$	0.0154	0.1656	0.786

312

313 Multiple comparison tests were performed to investigate the precise nature of the effects found to be
 314 significant in the ANOVA. Figure 5 shows the results of independent t-tests (significance indicated by #)
 315 comparing Δ OR to zero in each of the phase and amplitude levels. Only phase bins 90° and 270° in the
 316 high amplitude condition were found to be significantly different [$t(19) = -5.632, p = 0.0002$; $t(19) =$
 317 $3.466, p = 0.0207$ respectively, Bonferroni corrected for eight comparisons (Bland and Altman, 1995)].
 318 Tukey's HSD tests (indicated by *) then compared Δ OR distributions between phase bins within each
 319 amplitude level. These tests found significant differences in the phase bins only in the high amplitude
 320 condition. Specifically, the 90° phase bin was statistically different from the 0° ($p = 0.0077$), 180° ($p =$
 321 0.0308), and 270° ($p < 0.0001$) phase bins in the high amplitude condition (Figure 5). Importantly, the
 322 greatest difference in the high amplitude condition was found between phase bins 90° and 270°, with a
 323 22.20% increase in observation rates (95% CI = [9.77% , 34.63%], Figure 5). Collectively, these results

324 show that stimuli are observed with greatest probability when the alpha wave is near a trough at t_2 , and
325 with lowest probably when near a peak, when alpha amplitude is high. The perception-phase relationship
326 is robust only at high alpha wave amplitude, likely because during low amplitude oscillations the
327 measured phase is less representative of the underlying neural population activity.

328 *Phase-varying analysis of visual observation*

329 For a high-resolution characterization of the phase effect on Δ OR, we repeated the original procedure at
330 t_2 using 90° phase bins rotated in 1° increments for all 360° phase angles. Figure 6 shows Δ OR for each
331 of the twenty participants in both the high and low amplitude conditions as a function of the centered
332 alpha phase angle of the bins. Indicated along the circumference is the direction of the center of mass of
333 these phase diagrams for each condition, calculated as the angle of the vector mean of each of the 360
334 points forming the Δ OR distribution. This angle is referred to here as the preferred phase and indicates the
335 phase at which stimuli have the highest probability of being observed given the whole distribution. Note
336 that in the high amplitude condition, the preferred phase is between 180° and 360° (the negative-
337 amplitude portion of the alpha cycle) in 18/20 participants. These preferred phase angles have associated
338 magnitudes indicating how far the distribution's center of mass is offset in that direction and the strength
339 of the effect of phase on observation rates. These preferred phase angles and magnitudes for all
340 participants are shown in Figure 7, panels B and D.

341 Figure 7, panels A and C, show the Δ OR distributions averaged across all participants. Indicated in black
342 along the circumference is the group's preferred phase. Note that calculating the group's preferred phase
343 as the direction to the center of mass of the group's Δ OR distributions (Figure 7, panels A and C) is
344 equivalent to calculating the vector mean of the twenty individual preferred phases and associated
345 magnitudes (Figure 7, panels B and D). By taking the Δ OR value at the preferred phase angle and
346 subtracting from it the corresponding opposite phase angle (by 180° , referred to as the pessimal phase),
347 we calculated the preferred phase effect (PPE), which indicates the increase in observation rate from
348 pessimal to preferred alpha phase angles, relative to t_2 . Our results showed that the preferred phase was

349 similar in both the high and low amplitude conditions (272.41° and 284.65° , respectively) with a PPE of
350 20.96% in the high amplitude condition but 9.12% in the low amplitude condition. These data further
351 substantiate an interaction effect on observation probability between alpha wave phase and amplitude,
352 which was observed in the prior ANOVA analysis.

353 Additionally, we estimated the 95% confidence intervals (CI) for the group's preferred phase, which are
354 shown as the shaded regions along the circumference of the phase diagrams in Figure 7. These CIs could
355 only be estimated since there is not a known method of computing an angular CI on *non-unit* vectors
356 directly. To estimate these CIs, the twenty individual preferred phase vectors (with associated
357 magnitudes) were first converted to cartesian values. Then, two 95% CIs were calculated separately on
358 both the X and Y components, indicated respectively as the width and height of the shaded rectangles in
359 Figure 7, panels B and D. The angular interval that encompassed both CIs was then used to represent the
360 estimated 95% CI on the preferred phase in the polar space, although this interval will not necessarily be
361 centered on the preferred phase (i.e., mean). In the high amplitude condition, this resulted in an estimated
362 95% CI of $[234.75^\circ, 309.84^\circ]$, and in the low amplitude condition a much wider CI of $[206.22^\circ, 344.45^\circ]$.
363 Together with Figure 7A and B, these results show that observations rates are highest at the trough of the
364 alpha wave, and lowest at the peak. This effect is prominent in the high amplitude condition, but also to a
365 much lesser extent in the low amplitude condition recalling these effects did not reach significance in the
366 prior ANOVA.

367

368 ***Measuring induced activity***

369 Alpha band desynchronization (ERD) and phase resetting are characteristically observed in response to
370 relevant visual stimuli ([Klimesch et al., 2011](#)). These reflect neural processes resulting from the stimulus,
371 not spontaneous activity, and so in our case are only expected in response to observed trials, not missed
372 trials. To ensure that the amplitude and phase measurements made here are the result of spontaneous brain

373 activity and not caused by the stimulus itself, we verified that a drop in amplitude or sudden change in
374 phase coherence across trials does not occur in the observed trials at t_2 . Thus, we first calculated the
375 percent change in alpha amplitude, relative to a prestimulus baseline period of -300 to -100 ms, for both
376 the observed and missed trials and these are shown in Figure 8A. There was the expected characteristic
377 drop in alpha amplitude (i.e. ERD) in response to the observed stimuli, however this was not observed
378 until after 100 ms post stimulus which did not drop below that of the missed stimuli until after 200 ms.
379 This result indicates that measurements made at t_2 (whose mean value is 75.56 ms and range = [62.99,
380 88.87] ms) were safe from stimulus induced amplitude effects.

381 To ensure that there was no event related phase resetting, we next calculated phase coherence across all
382 trials, as well as just the observed and missed trials (Figure 8B). As shown in Figure 8B, no phase
383 resetting was apparent in the observed trials or in all trials together, especially prior to 150 ms. No event
384 related phase resetting would be expected in the missed trials, and this was not seen. However, in the
385 phase coherence across missed trials, there is a prominent peak measured at the 70.31 ms time point,
386 marked by the arrow in Figure 8B, but this not an event related phase reset as will be described further in
387 the Discussion. In sum, Figure 8 confirmed that no event related amplitude change or phase reset occurred
388 prior to 100 ms post stimulus, demonstrating that the phase and amplitude measurements taken in the
389 present study are not the result of stimulus induced activity, but of ongoing spontaneous oscillations.

390

391 ***t_2 measurements versus prestimulus measurements***

392 To evaluate the benefit of using the individual t_2 time point for measuring the alpha phase effect on
393 perceptual performance, we repeated the above analysis at a time point 100 ms prior to stimulus onset (t =
394 -100ms) and compared the results to those obtained above at t_2 . These measurements have been taken in
395 previous studies in prestimulus periods or at stimulus onset in order to avoid measuring induced
396 oscillatory effects as mentioned above ([Mathewson et al., 2009](#); [Mathewson et al., 2012](#); [Milton and](#)

397 Pleydell-Pearce, 2016; Kizuk and Mathewson, 2017). Whereas in the previous analysis, the four phase
 398 bins centered at 0°, 90°, 180°, and 270° were chosen *a priori* based on their theoretical significance at the
 399 *t2* time point, no prediction could be made about the relevant phase bins at this prestimulus time point.
 400 Instead, the analysis was first performed in 90° phase bins in 1° increments, as was performed previously
 401 (i.e. in Figure 7), and the four relevant phase bins were chosen empirically based on the observed
 402 preferred phase in the high amplitude condition. In other words, the phase bins were chosen *post hoc* in
 403 order to reveal the highest effect phase has on amplitude for this prestimulus *t* = -100ms time point.

404 The results of this analysis performed over all 90° bins in both the high and low amplitude conditions are
 405 shown in Figure 9. In the high amplitude condition, a phase effect on perceptual performance can again
 406 be observed, however in this case the preferred phase was measured at 33.53° (95% CI = [-31.69°,
 407 80.29°]) with a 15.48% PPE. In the low amplitude condition, the preferred phase was measured at -17.22°
 408 (95% CI = [-90.04°, 90.07°]) with a 5.22% PPE. Based on the preferred phase measured in the high
 409 amplitude condition for prestimulus *t* = -100ms, the four 90° phase bins centered at 33°, 123°, 213°, and
 410 303° were therefore chosen for the 2x4 repeated measures ANOVA analysis. Mauchly tests indicated no
 411 significant violation in the assumption of sphericity for phase ($\chi^2(5) = 5.194, p = 0.3926$), or the
 412 interaction of phase and amplitude ($\chi^2(5) = 8.861, p = 0.1147$). As shown in Table 2, only the main effect
 413 of phase was found to have a statistically significant effect on observation rates. Despite these phase bins
 414 showing the highest phase effects at *t* = -100ms, phase – whose bins were chosen *a priori* based on
 415 theoretical significance – had stronger effects on observation when the measurements were taken at *t2*
 416 (with roughly twice the effect size).

417

Table 2. Two (amplitude) x Four (phase) within-subjects repeated measures ANOVA results repeated at 100 ms prior to stimulus onset.

Source	Statistic	<i>p</i>	η_p^2	Power
--------	-----------	----------	------------	-------

phase	F(3,57) = 3.378	0.0243	0.1510	0.735
amplitude	F(1,19) = 0.008	0.9289	0.0004	0.051
phase*amplitude	F(3,57) = 1.695	0.1784	0.0819	0.420

418

419 Figure 10 shows the multiple comparisons result for this data collected at 100 ms prior to stimulus onset
 420 for better comparison to those from $t2$ shown in Figure 5. Bonferroni corrected independent t-tests
 421 compared each Δ OR value to zero, but none were found to be significant, indicating that none of the
 422 observation rates in any of these four phase bins differed from the overall mean observation rate either
 423 amplitude condition. Tukey's HSD tests (indicated by *) were used to compare Δ OR distributions
 424 between phase bins within each amplitude level, but these tests only found a significant difference
 425 between 33° and 213° ($p = 0.0143$) where there was a 15.47% difference in observations rates (95% CI =
 426 [2.39%, 28.55%]).

427 In our original hypothesis, we predicted that the high amplitude preferred phase would be 270° at $t2$,
 428 which was approximately $t=75$ ms on average. Assuming 1) a perfectly stationary and 2) an exactly 10Hz
 429 signal, we would have predicted that the preferred phase at $t=-100$ ms, as well as at $t0$, would have been
 430 0°. This was approximately what was found here, however the inexactness is expected since neither
 431 assumption is exactly met in the natural alpha rhythm. The non-stationarity would additionally explain the
 432 decrease in effect size from $t2$ to $t=-100$ ms. Collectively, these results show that although an alpha phase
 433 effect on observation rates in a prestimulus period can be observed, the strength of the effect is much
 434 weaker than when measurements are taken at $t2$. This finding shows that measurement of alpha
 435 oscillations amplitude and phase have the strongest correlation with visual perception at $t2$ than at $t=-100$
 436 ms.

437 **Discussion**

438 This study presents a novel, controlled method for examining the neuronal shutter effect, hypothesized to
439 be reflected in the posterior alpha oscillations observed in human EEG. Our hypothesis was that
440 perceptual performance is modulated by the alpha rhythm in a precise phase and timing relationship. To
441 test this relationship, we (1) presented near-threshold intensity visual stimuli through closed eyes to
442 participants; (2) accounted for individual retina-to-V1 conduction delays (t_2); (3) controlled for
443 asynchrony between hemispheres; and (4) measured the alpha phase and amplitude relative to t_2 . Our
444 results confirm the hypothesized relationship between the alpha rhythm phase and perception, with the
445 greatest rates of observation occurring at the alpha wave trough (excitatory state) and the lowest rates at
446 the alpha wave peak (inhibitory state). The perception-phase relationship appears to be modulated by
447 alpha amplitude as it is observed at high, but not low, alpha wave amplitude. This work is novel in
448 considering the underlying neural structure and function of the visual system when predicting the exact
449 phase relationship to perception, and in controlling for individual neural conduction delay and asynchrony
450 between hemispheres.

451 While the alpha wave shutter effect has been previously examined ([Dustman and Beck, 1965](#); [Mathewson](#)
452 [et al., 2009](#); [Mathewson et al., 2012](#); [Milton and Pleydell-Pearce, 2016](#); [Kizuk and Mathewson, 2017](#)),
453 this is the first study, to our knowledge, to directly examine the relationship between perceptual
454 performance and spontaneous alpha phase as measured relative to each individual's conduction delay.
455 Previous studies have either measured alpha phase at stimulus onset, t_0 , or during prestimulus
456 periods ([Mathewson et al., 2009](#); [Mathewson et al., 2012](#); [Milton and Pleydell-Pearce, 2016](#); [Kizuk and](#)
457 [Mathewson, 2017](#)). Accordingly, the phase measurements were not always well aligned with the LGN
458 excitability state according to the proposed cellular mechanism. Here, when we accounted for each
459 individual's conduction delay, as opposed to the group average conduction delay or measuring at stimulus
460 onset t_0 , we demonstrated the existence of a hypothesized relationship between the alpha phase and
461 perception. Notably, these results provide the most robust evidence consistent with cyclic LGN

462 excitability as the cellular mechanism mediating this effect – though we do not directly examine observe
463 this mechanism. Dustman and Beck (1965) measured reactions times, as opposed to observation rates, at
464 alpha phase adjusted to group average, as opposed to individual conduction delay. This study, similar to
465 ours, found slowest reaction times at the peak (90°) of the alpha wave, and fastest reaction times close to
466 the alpha trough (240°).

467 A 2x4 repeated measures ANOVA found that alpha phase at t_2 had a significant effect on perceptual
468 performance as hypothesized. The interaction effect of phase and amplitude was also found to be
469 significant; the multiple comparisons tests in Figure 5 show that low amplitude attenuates the phase
470 effect. This supports the hypothesis that low amplitude alpha waves reflect asynchronous inhibition
471 within the visual system. Although not part of our original hypothesis, it is somewhat surprising that no
472 main effect of amplitude was found since increased alpha power has sometimes been found to predict
473 poorer perceptual performance (Ergenoglu et al., 2004; Mathewson et al., 2009; Bruers and VanRullen,
474 2018). This perception-power relationship is usually attributed to more generalized early visual inhibition
475 as evidenced by the attenuation of early (C1 and N150) VEP components with increased alpha power
476 (Iemi et al., 2019). Figure 7 gives a higher phase angle resolution view of the effects seen in Figure 5. In
477 both the high and low amplitude conditions, the preferred phase was near the wave trough (272.41° and
478 284.65° at high and low amplitude, respectively). However, in the low amplitude condition, the 95% CI
479 of the preferred phase was much wider, and the PPE was lower (20.96% and 9.12% at high and low
480 amplitude, respectively). These results show how alpha amplitude modulates the effect of alpha phase on
481 perception.

482 To demonstrate the significance of taking alpha amplitude and phase measurements at t_2 , we repeated our
483 analysis at $t = -100$ ms and compared them to those obtained at t_2 . This prestimulus time point was chosen
484 for two reasons. First, given the risk in poststimulus measurements getting altered by stimulus processing,
485 a prestimulus time point is, therefore, “safer” than a post-stimulus or stimulus-onset time points. Second,
486 given that alpha oscillations have a primary frequency of 10Hz (i.e., has a period of 100ms), the

487 amplitude-phase relationship would repeat roughly every 100ms. Thus, our results at $t = -100$ ms could
488 help to predict this relationship at stimulus onset, which is 100ms (or one period) away, but under safer
489 signal analysis conditions. At prestimulus time point of -100 ms ($t = -100$ ms), we did find a significant
490 phase effect, but by using different phase bins more relevant to that time point (i.e., 33° , 123° , 213° ,
491 360°). These phase bins were chosen *post hoc* to reveal the highest effect phase has on observation for
492 this prestimulus time point. Despite showing the highest phase effects, phase – whose bins were chosen *a*
493 *priori* based on theoretical significance – had stronger effects on observation when the measurements
494 were taken at t_2 . Specifically, the new analysis shows that while phase was found to have a statistically
495 significant effect on observation rates between the preferred and pessimal phase bins in the high
496 amplitude condition, the effect size was weaker and roughly half of that at t_2 . These results show the
497 advantage of making phase and amplitude measurements at t_2 rather than in prestimulus periods.

498 Poststimulus measures of ongoing spontaneous oscillations are generally avoided since there is a risk that
499 they will be altered by stimulus processing. We verified that our t_2 amplitude and phase measurements
500 were not influenced by that by measuring alpha band ERD/S and ITPC over the -300 to 500ms time range
501 relative to stimulus onset (Figure 8). No stimulus related ERD/S or ITPC were observed prior to 100ms
502 indicating that our measures at t_2 were independent of stimulus processing responses and instead reflected
503 spontaneous activity. Interestingly, there was an overall increase in phase coherence values of the
504 observed and missed trials compared to that of all trials combined (Figure 7B). This increase is expected
505 since, according to the phase effects on observation rates found above, trials that are observed and missed
506 will predominantly occupy specific, opposing phase ranges; thereby resulting in relatively high phase
507 coherence across trials when grouped by observational outcome, and low phase coherence when grouped
508 together. It is also important to note that the missed trial phase coherence trace features a prominent peak
509 at 70.41 ms (indicated by the arrow in Figure 8B). We do not interpret this peak as an event related phase
510 reset since 1) it is the peak of an upward trend beginning at least 300 ms prior to stimulus onset, 2) a
511 decreasing trend is observed immediately afterwards, and 3) no phase reset would be expected in response

512 to an unobserved stimulus. Instead, we interpret this peak as probably marking the time where phase most
513 accurately predicts that a stimulus will not be observed, which – in support of our hypothesis – is within 5
514 ms of the average estimated t_2 (75.56 ms), the point hypothesized to best predict observational outcome.

515 *Neural mechanism*

516 Understanding the biological mechanism underlying alpha oscillation is important for explaining its
517 function. Although simultaneous recordings with fMRI and PET correlated alpha activity with
518 fluctuations in the thalamus, thus suggesting this might be the origin of alpha rhythm (Hughes et al.,
519 2004; Omata et al., 2013), so far the precise mechanism in humans is not yet agreed on. However, sleep
520 spindles, a ~10 Hz alpha-like oscillation that occurs in 1-3 second bursts during transition to sleep, do
521 have a well-established mechanism. The sleep spindle mechanism includes a negative feedback loop
522 between the LGN and the reticular nucleus (RN, shown in Figure 11). Both nuclei have T-type Ca^+
523 channels that, when activated, exhibit burst firing. Between each burst of the LGN, the Ca^+ channels of
524 the LGN are known to enter a refractory period, and the RN sends a similar, but inhibitory, burst to the
525 LGN. During this time, sensory information from the optic nerve would be less likely to be relayed to V1.
526 Importantly, the refractory periods of these T-type Ca^+ channels are known to result in each nucleus firing
527 at a ~10 Hz rate (Lopes da Silva, 1991; Sherman, 2001; Timofeev and Bazhenov, 2005; Alexander et al.,
528 2006; Timofeev and Chauvette, 2011). Each LGN burst firing generates massive EPSPs in V1, measured
529 as a negativity in the occipital EEG (Timofeev and Bazhenov, 2005) and producing the ~10 Hz oscillation
530 of sleep spindles seen on EEG. Chen et al. (2016) showed that in mice, very similar mechanisms give rise
531 to both sleep spindles *and* waking alpha oscillations, and that the mechanism is capable of phasically
532 modulating sensory transfer through the thalamus, and on this basis, they predicted the perceptual results
533 found here. In cats, this mechanism was also found to produce waking alpha oscillations with the same
534 phasic sensory gating effect (Lorincz et al., 2009). Although additional and alternate sources, including
535 extrastriate cortical sources, have been proposed to give rise to this oscillatory activity (Steriade et al.,
536 1990; Connors and Amitai, 1997; Bollimunta et al., 2008; van Dijk et al., 2008; Bollimunta et al., 2011),

537 there is much evidence supporting this thalamic mechanism as the primary driver (Hughes and Crunelli,
538 2005). Although the present study does not directly test this thalamic mechanism, it is offered as a purely
539 speculative explanation for our results on the basis of previous and more direct research findings (Lorincz
540 et al., 2009; Chen et al., 2016).

541

542 ***Cellular shutter effect generates a behavioral graded gating effect***

543 Although our speculation and not directly tested here, if the neural mechanism posited above were
544 correct, the neuron shutter effect would then best be described as occurring at the level of individual
545 LGN relay cells, in which the effect may occur at a nearly binary level. However, the behavioral effects
546 we observe are graded, with increasing and decreasing probabilities of stimulus observation. This may be
547 explained given that oscillating excitatory states are not always synchronized across all LGN cells. It is
548 not necessarily the case that all cells are simultaneously in burst-mode firing state; some may
549 concurrently operate in the normal tonic firing state. Thus, one cell may be in a state of inhibition and not
550 relay to V1, while others may relay visual information as usual. However, in asynchronous states, the
551 alpha rhythm should be decreased in amplitude. As shown in this study, at higher alpha amplitudes, the
552 differences in observation rates between peak and trough phases at t_2 increased, presumably indicating
553 that the measured phase becomes more representative of the excitatory state of larger populations of LGN
554 cells with increasing alpha amplitude. Asynchrony is also important to consider, not just among cells
555 within an LGN, but between the LGNs of the left and right hemispheres. As on a cellular level, one LGN
556 may restrict the flow of visual information while the other relays it. Presumably, if all cells within and
557 between LGNs were in perfect synchrony, behavior relative to peak/trough phase at t_2 would reflect a
558 perfect on/off visual shutter. This simple relationship wasn't observed in this study, and it is therefore
559 more appropriate to describe the proposed neuron shutter effect at the cellular level generating a graded,
560 gating effect of perception at the behavioral level.

561

562 In sum, to our knowledge, this is the first study to examine the neuronal shutter effect with an exact phase
563 and timing relationship to perceptual performance predicted by the underlying physiology of the visual
564 system. The study design is novel and rigorous in controlling for individual visual conduction delays and
565 hemispheric asynchrony. During times of high amplitude alpha oscillations, we found participants on
566 average are most likely to perceive stimuli at waveform trough (272.41°) with observation rates 20.96%
567 greater than at the opposing peak phase (92.41°). Given the rigor in our phase measurements, these results
568 provide strong support for a mechanism that modulates perception described by the neuronal shutter
569 effect and is reflected in the posterior alpha rhythm. Further studies with conduction delay-adjusted phase
570 measurement are needed to investigate this shutter effect in the mu and tau rhythms over the sensorimotor
571 and auditory cortices, to explore the possibility of this mechanism in other sensory systems.

572 **References**

- 573 Alexander GM, Carden WB, Mu J, Kurukulasuriya NC, McCool BA, Nordskog BK, Friedman DP,
574 Daunais JB, Grant KA, Godwin DW (2006) The Native T-Type Calcium Current in Relay
575 Neurons of The. *Neuroscience* 141:453-461.
- 576 American Electroencephalographic Society (1994) Guideline thirteen: guidelines for standard electrode
577 position nomenclature. American Electroencephalographic Society. *J Clin Neurophysiol* 11:111-
578 113.
- 579 Ancoli S, Green KF (1977) Authoritarianism, Introspection, and Alpha Wave Biofeedback Training.
580 *Psychophysiology* 14:40-44.
- 581 Barry RJ, Clarke AR, Johnstone SJ, Magee CA, Rushby JA (2007) EEG differences between eyes-closed
582 and eyes-open resting conditions. *Clinical Neurophysiology* 118:2765-2773.
- 583 Bazanova OM, Vernon D (2014) Review: Interpreting EEG alpha activity. *Neuroscience and*
584 *Biobehavioral Reviews* 44:94-110.
- 585 Ben-Simon E, Podlipsky I, Okon-Singer H, Gruberger M, Cvetkovic D, Intrator N, Hendler T (2013) The
586 Dark Side of the Alpha Rhythm: fMRI Evidence for Induced Alpha Modulation During Complete
587 Darkness. *European Journal of Neuroscience* 37:795-803.
- 588 Berens P (2009) CircStat: A MATLAB Toolbox for Circular Statistics. *Journal of Statistical Software*
589 31:21.
- 590 Berry RB, Wagner MH (2015) *Sleep Medicine Pearls*, 3 Edition: Elsevier/Saunders.
- 591 Bierings RAJM, Kuiper M, Van Berkel CM, Overkempe T, Jansonius NM (2018) Foveal Light and Dark
592 Adaptation in Patients With Glaucoma and Healthy Subjects: A Case-Control Study. *PLoS ONE*
593 13.
- 594 Bland JM, Altman DG (1995) Multiple Significance Tests: The Bonferroni Method. *BMJ: British*
595 *Medical Journal* 310:170-170.
- 596 Bollimunta A, Chen Y, Schroeder CE, Ding M (2008) Neuronal mechanisms of cortical alpha oscillations
597 in awake-behaving macaques. *J Neurosci* 28:9976-9988.

- 598 Bollimunta A, Mo J, Schroeder CE, Ding M (2011) Neuronal mechanisms and attentional modulation of
599 corticothalamic alpha oscillations. *J Neurosci* 31:4935-4943.
- 600 Brainard DH (1997) The Psychophysics Toolbox. *Spatial Vision* 10:433-436.
- 601 Bruers S, VanRullen R (2018) Alpha Power Modulates Perception Independently of Endogenous Factors.
602 *Frontiers in Neuroscience* 12:279.
- 603 Callaway E, Alexander JD (1960) The Temporal Coding of Sensory Data: An Investigation of Two
604 Theories. *Journal of General Psychology* 62:293-309.
- 605 Chen Z, Wimmer RD, Wilson MA, Halassa MM (2016) Thalamic Circuit Mechanisms Link Sensory
606 Processing in Sleep and Attention. In, pp 83-83.
- 607 Clark VP, Fan S, Hillyard SA (1995) Identification of Early Visual Evoked Potential Generators by
608 Retinotopic and Topographic Analyses. *Human Brain Mapping* 2:170-187.
- 609 Cohen MX (2014) *Analyzing Neural Time Series Data: Theory and Practice*: MIT Press.
- 610 Cohen MX (2019) A Better Way to Define and Describe Morlet Wavelets for Time-Frequency Analysis.
611 *NeuroImage* 199:81-86.
- 612 Connors BW, Amitai Y (1997) Making waves in the neocortex. *Neuron* 18:347-349.
- 613 Cooper NR, Croft RJ, Dominey SJJ, Burgess AP, Gruzelier JH (2003) Paradox Lost? Exploring the Role
614 of Alpha Oscillations During Externally vs Internally Directed Attention and the Implications for
615 Idling and Inhibition Hypotheses. *International Journal of Psychophysiology* 47:65-74.
- 616 Cornsweet TN (1962) The Staircase Method in Psychophysics. *The American Journal of Psychology*
617 75:485-491.
- 618 Delorme A, Makeig S (2004) EEGLAB: an Open Source Toolbox for Analysis of Single-Trial EEG
619 Dynamics Including Independent Component Analysis. *Journal of Neuroscience Methods* 134:9-
620 21.
- 621 Di Russo F, Martínez A, Sereno MI, Pitzalis S, Hillyard SA (2001) Cortical Sources of the Early
622 Components of the Visual Evoked Potential. *Human Brain Mapping* 15:95-111.

- 623 Dustman RE, Beck EC (1965) Phase of Alpha Brain Waves, Reaction Time and Visually Evoked
624 Potentials. *Electroencephalogr Clin Neurophysiol* 18:433-440.
- 625 Ergenoglu T, Demiralp T, Bayraktaroglu Z, Ergen M, Beydagi H, Uresin Y (2004) Alpha rhythm of the
626 EEG modulates visual detection performance in humans. *Cognitive Brain Research* 20:376-383.
- 627 Gonçalves SI, de Munck JC, Pouwels PJW, Schoonhoven R, Kuijer JPA, Maurits NM, Hoogduin JM,
628 Van Someren EJW, Heethaar RM, Lopes da Silva FH (2006) Correlating the alpha rhythm to
629 BOLD using simultaneous EEG/fMRI: Inter-subject variability. *Neuroimage* 30:203-213.
- 630 Hughes SW, Crunelli V (2005) Thalamic mechanisms of EEG alpha rhythms and their pathological
631 implications. In, pp 357-372.
- 632 Hughes SW, Lorincz M, Cope DW, Blethyn KL, Kekesi KA, Parri HR, Juhasz G, Crunelli V (2004)
633 Synchronized Oscillations at Alpha and Theta Frequencies in the Lateral Geniculate Nucleus. In,
634 pp 253-268: *Neuron*.
- 635 Iemi L, Busch NA, Laudini A, Haegens S, Samaha J, Villringer A, Nikulin VV (2019) Multiple
636 mechanisms link prestimulus neural oscillations to sensory responses. *Elife* 8.
- 637 Janssens C, De Loof E, Nico Boehler C, Pourtois G, Verguts T (2018) Occipital Alpha Power Reveals
638 Fast Attentional Inhibition of Incongruent Distractors. *Psychophysiology* 55:1-11.
- 639 Kizuk SA, Mathewson KE (2017) Power and Phase of Alpha Oscillations Reveal an Interaction between
640 Spatial and Temporal Visual Attention. *J Cogn Neurosci* 29:480-494.
- 641 Kleiner M, Brainard D, Pelli D, Ingling A, Murray R, Broussard C (2007) What's New in Psychtoolbox-3.
642 In, pp 1-16.
- 643 Klimesch W, Fellinger R, Freunberger R (2011) Alpha oscillations and early stages of visual encoding.
644 *Front Psychol* 2:118.
- 645 Legewie H, Simonova O, Creutzfeldt OD (1969) EEG changes during performance of various tasks under
646 open- and closed-eyed conditions. *Electroencephalography & Clinical Neurophysiology* 27:470-
647 479.

- 648 Lopes da Silva F (1991) Neural Mechanisms Underlying Brain Waves: From Neural Membranes.
649 Electroencephalography and Clinical Neurophysiology 79:81-93.
- 650 Lopez-Calderon J, Luck SJ (2014) ERPLAB: An Open-Source Toolbox for the Analysis of Event-Related
651 Potentials. *Frontiers in Human Neuroscience* 8.
- 652 Lorincz ML, Kekesi KA, Juhasz G, Crunelli V, Hughes SW (2009) Temporal framing of thalamic relay-
653 mode firing by phasic inhibition during the alpha rhythm. *Neuron* 63:683-696.
- 654 Mathewson KE, Gratton G, Fabiani M, Beck DM, Ro T (2009) To See or Not to See: Prestimulus Alpha
655 Phase Predicts Visual Awareness. *Journal Of Neuroscience* 29:2725-2732.
- 656 Mathewson KE, Prudhomme C, Fabiani M, Beck DM, Lleras A, Gratton G (2012) Making Waves in the
657 Stream of Consciousness: Entraining Oscillations in EEG Alpha and Fluctuations in Visual
658 Awareness With Rhythmic Visual Stimulation. *Journal Of Cognitive Neuroscience* 24:2321-
659 2333.
- 660 Milton A, Pleydell-Pearce CW (2016) The phase of pre-stimulus alpha oscillations influences the visual
661 perception of stimulus timing. *Neuroimage* 133:53-61.
- 662 Omata K, Hanakawa T, Morimoto M, Honda M (2013) Spontaneous Slow Fluctuation of EEG Alpha
663 Rhythm Reflects Activity in Deep-Brain Structures: A Simultaneous EEG-fMRI Study. *PLoS*
664 *ONE* 8:1-12.
- 665 Pelli DG (1997) The VideoToolbox software for visual psychophysics: Transforming numbers into
666 movies. *Spatial Vision* 10:437-442.
- 667 Pfurtscheller G, Stancák A, Jr., Neuper C (1996) Event-related synchronization (ERS) in the alpha band--
668 an electrophysiological correlate of cortical idling: a review. *International journal of*
669 *psychophysiology : official journal of the International Organization of Psychophysiology* 24:39-
670 46.
- 671 Pineda JA (2005) The Functional Significance of Mu Rhythms: Translating “Seeing” and “Hearing” Into
672 “Doing”. *Brain Research Reviews* 50:57-68.

- 673 Ray WJ, Cole HW (1985) EEG Alpha Activity Reflects Attentional Demands, and Beta Activity Reflects
674 Emotional and Cognitive Processes. *Science* 228:750-752.
- 675 Sauseng P, Klimesch W, Stadler W, Schabus M, Doppelmayr M, Hanslmayr S, Gruber WR, Birbaumer N
676 (2005) A Shift of Visual Spatial Attention is Selectively Associated With Human EEG Alpha
677 Activity. *The European Journal Of Neuroscience* 22:2917-2926.
- 678 Seeck M, Koessler L, Bast T, Leijten F, Michel C, Baumgartner C, He B, Beniczky S (2017) The
679 standardized EEG electrode array of the IFCN. *Clin Neurophysiol* 128:2070-2077.
- 680 Sherman SM (2001) Tonic and Burst Firing: Dual Modes of Thalamocortical Relay. *TRENDS in*
681 *Neurosciences* 24:122-126.
- 682 Steriade M, Gloor P, Llinas RR, Lopes de Silva FH, Mesulam MM (1990) Basic mechanisms of cerebral
683 rhythmic activities. *Electroencephalogr Clin Neurophysiol* 76:481-508.
- 684 Tenke CE, Kayser J, Svob C, Miller L, Alvarenga JE, Abraham K, Warner V, Wickramaratne P,
685 Weissman MM, Bruder GE (2017) Association of Posterior EEG Alpha With Prioritization of
686 Religion or Spirituality: A Replication and Extension at 20-Year Follow-Up. *Biological*
687 *Psychology* 124:79-86.
- 688 Tiihonen J, Hari R, Kajola M, Karhu J, Ahlfors S, Tissari S (1991) Magnetoencephalographic 10-Hz
689 Rhythm From the Human Auditory Cortex. *Neuroscience Letters* 129:303-305.
- 690 Timofeev I, Bazhenov M (2005) Mechanisms and Biological Role of Thalamocortical Oscillations.
- 691 Timofeev I, Chauvette S (2011) Thalamocortical Oscillations: Local Control of EEG Slow Waves.
692 *Current Topics in Medicinal Chemistry* 11:2457-2471.
- 693 van Dijk H, Schoffelen JM, Oostenveld R, Jensen O (2008) Prestimulus oscillatory activity in the alpha
694 band predicts visual discrimination ability. *J Neurosci* 28:1816-1823.
- 695 VanRullen R, Koch C (2003) Is perception discrete or continuous? *Trends in Cognitive Sciences* 7:207-
696 213.
- 697 VanRullen R, Zoefel B, Ilhan B (2014) On the cyclic nature of perception in vision versus audition.
698 *Philos Trans R Soc Lond B Biol Sci* 369:20130214.

- 699 Weisz N, Hartmann T, Müller N, Lorenz I, Obleser J (2011) Alpha Rhythms in Audition: Cognitive and
700 Clinical Perspectives. *Frontiers in Psychology* 2:1-15.
- 701 Wieneke GH, Deinema CH, Spoelstra P, Storm van Leeuwen W, Versteeg H (1980) Normative spectral
702 data on alpha rhythm in male adults. *Electroencephalography and clinical neurophysiology*
703 49:636-645.
- 704 Yue W, Chun NW, Siong NK, Tiecheng W, Xiaoping L (2013) An EEG Source Localization and
705 Connectivity Study on Deception of Autobiography Memories. In, pp 468-471: IEEE.

706 **Legends**

707

Figure 1. (A) According to the cruciform model of the calcarine fissure in the V1 cortical area, the lower portion of the fissure will respond to upper visual field stimuli and vice versa for the upper portion of the fissure. For this reason, and as the upper and lower portions of the fissure contain opposing dipoles, upper and lower visual field stimuli will create waveforms of opposing polarity in the EEG. (B) Upper and lower visual field stimuli used for C1 VEP task are centered 3° below the fixation point to account for the overrepresentation of the lower visual field in the calcarine fissure as shown in (A). (C) C1 VEP from a single participant in response to the upper and lower stimuli, the difference was measured as the lower minus the upper VEP. The peak latency of the difference wave (indicated as '+') was used as the estimate of t_2 .

708

Figure 2. Example of the staircase method used to determine the threshold intensity in a single participant. Each time the participant observed the stimulus, the intensity in the next trial was decreased. If the participant did not observe the stimulus in one trial, the intensity was increased in the next trial. Threshold intensity was determined as the average intensity of all trials (trials 6-40 in this example) following the third reversal, or corner, in the trial-intensity trace (trial 5 in this example). The dashed threshold intensity line in this figure spans the trials over which the intensities were averaged.

709

Figure 3. Each of the twenty participants' alpha peak-to-peak amplitude distribution for all trials used in the analysis at t_2 .

710

Figure 4. C1 VEP component averaged across all participants in response to upper and lower visual field stimuli. The ‘Difference’ waveform is the ‘Lower’ waveform subtracted from the ‘Upper’ waveform. The mean and range of each participant’s estimated retina-to-V1 conduction delay (t_2) is indicated and was calculated as the peak latency of the C1 component in each individual’s Difference waveform.

711

Figure 5. Mean change in observation rate (Δ OR) for each amplitude and phase condition relative to mean OR across all conditions when analysis was conducted at t_2 (error bars indicate standard error). Tukey’s HSD tests were performed between phase levels within amplitude conditions with significance indicated by ‘*’. Bonferroni corrected t-tests compared each mean to zero with significance indicated by ‘#’. $90^\circ = \text{peak}$. ([*.#]: $p \leq 0.05$, [**.#]: $p \leq 0.01$, [***.#]: $p \leq 0.001$, [****.###]: $p \leq 0.0001$)

712

Figure 6. Δ OR as a function of phase for each participant in the high and low amplitude conditions with radial axis extending to negative values for analysis conducted at $t2$. The preferred phase is indicated on the circumference, calculated as the direction towards the circle's center of mass. $90^\circ = \text{peak}$.

713

Figure 7. Analysis conducted at $t2$. Panels A and C show Δ OR as a function of phase, with radial axis extending to negative values. Panels B and D show individual participants' preferred phase angles; their magnitude is proportional their individual preferred phase effect. The width and height of the shaded rectangles indicate, respectively, the X and Y 95% CI in cartesian space. In all panels, the group mean preferred phase is indicated in black on the circumference of the diagrams, with the shaded region indicating estimated 95% CIs for each amplitude condition. $90^\circ = \text{peak}$.

714

Figure 8. (A) Change in alpha amplitude, relative to a -300 to -100 ms baseline interval, and (B) alpha phase coherence for observed, missed, and all stimuli together. The arrow indicates a peak in the missed trial phase coherence reflecting the time point where alpha phase best predicts that a trial will be unobserved by the participant. There was no indication of stimulus-induced effects at the t_2 time point where phase and amplitude measures were hypothesized to be of mechanistic relevance.

715

Figure 9. Analysis conducted at $t = -100$ ms. Panels A and C show Δ OR as a function of phase, with radial axis extending to negative values. Panels B and D show individual participants' preferred phase angles; their magnitude is proportional to their individual preferred phase effect. The width and height of the shaded rectangles indicate, respectively, the X and Y 95% CI in cartesian space. In all panels, the group mean preferred phase is indicated in black on the circumference of the diagrams, with the shaded region indicating estimated 95% CIs for each amplitude condition. $90^\circ = \text{peak}$.

716

Figure 10. Mean change in observation rate (Δ OR) for each amplitude and phase condition relative to mean OR across all conditions when analysis was conducted at $t = -100$ ms (error bars indicate standard error). Tukey's HSD tests were performed between phase levels within amplitude conditions with significance indicated by '*'. Bonferroni corrected did not find any of the means to significantly differ from zero. $90^\circ = \text{peak}$. (*: $p \leq 0.05$).

717

Figure 11. Visual pathway from retina to V1. The LGN/RN negative feedback loop provides a mechanism of cycling LGN excitability state. This LGN/RN network is known to give rise to sleep spindles. The same, or a similar, mechanism is expected to give rise the posterior alpha rhythm.

718

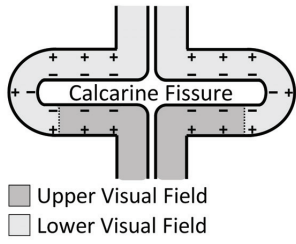
Table 1. Two (amplitude) x Four (phase) within-subjects repeated measures ANOVA results at $t= t2$.

719

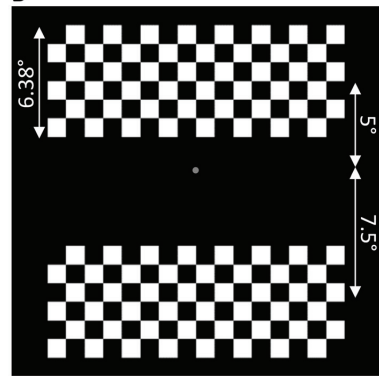
Table 2. Two (amplitude) x Four (phase) within-subjects repeated measures ANOVA results repeated at 100 ms prior to stimulus onset ($t= -100$ ms).

720

A



B



C

